PRECISE PREDICTIONS FOR $t\bar{t} + E_{\mathrm{T}}^{\mathrm{miss}}$ AT THE LHC*

Giuseppe Bevilacqua

MTA-DE Particle Physics Research Group, University of Debrecen
4010 Debrecen, P.O. Box 105, Hungary

(Received October 28, 2019)

Triggered by ongoing dark matter searches in the $t\bar{t} + E_{\mathrm{T}}^{\mathrm{miss}}$ channel, we present state-of-the-art predictions for the Standard Model background process $pp \to t\bar{t}Z(Z \to \nu\bar{\nu})$ with leptonic top-quark decays. Our calculation is accurate at next-to-leading order in QCD and includes for the first time off-shell and non-resonant effects for the decays of top quarks and heavy bosons. We show predictions for the LHC at 13 TeV for several observables of phenomenological interest, together with a full estimate of the theoretical uncertainties stemming from variation of scales and parton distribution functions.

DOI:10.5506/APhysPolB.50.1881

1. Introduction

Despite the spectacular success so far achieved, the Standard Model of particle physics (SM) leaves several important questions unanswered. Among others, it does not provide any viable dark matter (DM) candidate with all the required properties deduced from cosmological observations. The evidence for the existence of DM, although indirect, is quite convincing and is driving a very active program of research. Depending on the typology of experiment, the signal to look for may come from the interaction between DM and SM particles, or from the annihilation of DM particles into SM ones. The first kind of experiments aims at a direct detection, while the second one is designed to catch indirect signals. There is yet another type of search, where one looks for signals of DM production via annihilation of SM particles. The latter approach is typical of high-energy colliders like the currently operating LHC. Since DM particles do not interact with SM, they cannot be detected directly. The observation of events with a large amount of missing transverse energy ($E_{\mathrm{T}}^{\mathrm{miss}}$) is thus a typical signature of dark matter at colliders.

* Presented at the XLIII International Conference of Theoretical Physics "Matter to the Deepest", Chorzów, Poland, September 1–6, 2019.

Several theories predict candidate DM particles that could be produced at the LHC. They are massive and weakly interacting, so they escape detection. Supersymmetric neutralinos are well-known examples of such particles. Alternatively, one can study dark matter in the framework of simplified models [1] where it is assumed the existence of a mediator particle — whose CP nature is to be determined — that couples to both SM and DM sectors. The couplings of the mediator to the SM fermions are strongly constrained by precision flavor measurements. The hypothesis of Minimal Flavor Violation (MFV) is often invoked [2], according to which the coupling between any new neutral spin-zero state and SM fermions must be proportional to the fermion masses. Thus, in models with MFV, dark matter couples preferentially to top quarks. The process of top-quark pair production in association with missing energy ($t\bar{t} + E_{\mathrm{T}}^{\mathrm{miss}}$) is an interesting channel to search for.

Several SM processes play the role of backgrounds to $t\bar{t}$ + DM production at the LHC. Due to the presence of undetected neutrinos, the process $pp \to t\bar{t}Z(Z \to \nu\bar{\nu})$ represents an *irreducible* background. There are also sources of *reducible* background, such as $pp \to t\bar{t}$, $pp \to t\bar{t}W$, $pp \to WW/WZ/ZZ$ or $pp \to Z+$jets, which are relatively easier to control. A precise modeling of these processes, particularly of the $t\bar{t}Z$ background, is a key ingredient for determining the nature of the DM mediator in simplified models (see *e.g.* Ref. [4]). With this motivation at hand, we have performed a complete NLO QCD calculation for the SM process $pp \to t\bar{t}Z(Z \to \nu\bar{\nu})$ in the dilepton channel. This work improves the current state-of-the-art description of $t\bar{t}Z$ [7–13] by including for the first time complete off-shell and non-resonant effects for top-quarks, W- and Z-boson decays at NLO QCD accuracy. We report on the results of this calculation, as presented in [3].

2. Calculational framework

We perform an NLO QCD analysis of the process $pp \to b\bar{b}e^+\nu_e\mu^-\bar{\nu}_\mu\nu_\tau\bar{\nu}_\tau+X$ at the perturbative order $\mathcal{O}(\alpha^6\alpha_{\mathrm{s}}^3)$. This process entails the production of $t\bar{t}Z$ final states with leptonic top-quark decays and invisible decays for the Z boson, including off-shell and non-resonant effects. A few representative examples of Feynman diagrams contributing to the amplitude are shown in Fig. 1. All fermions with the exception of the top quark are considered massless. Due to the presence of unstable top quarks, the complex mass scheme [27] is adopted. Further technical details can be also found in our earlier work on $t\bar{t}$, $t\bar{t}j$ and $t\bar{t}\gamma$ production [28–32]. Scale uncertainties are estimated by varying the default values of the renormalization and factorization scales independently by a factor of 2 and taking the envelope of the resulting predictions. Following the PDF4LHC recommendations for LHC Run 2 [33], we consider the PDF sets CT14 [34], MMHT14 [35] and NNPDF3.0 [36] for our predictions.

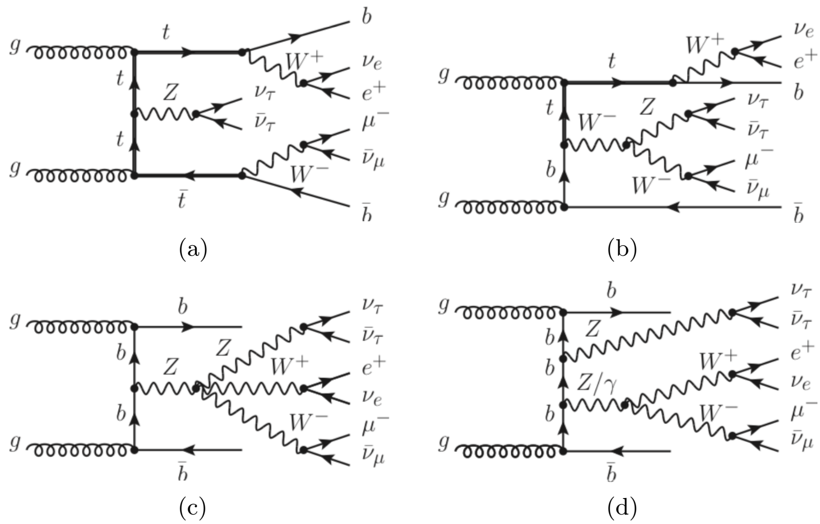

Fig. 1. Representative examples of double-resonant (a), single-resonant (b) and non-resonant (c), (d) diagrams entering the amplitude of the process $pp \to b\bar{b}e^+\nu_e\mu^-\bar{\nu}_\mu\nu_\tau\bar{\nu}_\tau$ at the leading order.

On the technical side, our results have been obtained with the help of the package HELAC-NLO [17], which comprises HELAC-1LOOP [18] and HELAC-DIPOLES [24, 25]. The virtual contributions are calculated according to the OPP method [14] using the programs CutTools [15] and OneLOop [16] as cornerstones. Real-emission contributions are calculated using the Nagy–Soper scheme [25] and cross-checked against Catani–Seymour subtraction [19, 20]. Phase space integration is performed by use of KALEU [21]. The final results are available in the form of events in either Les Houches Event File format [22] or ROOT Ntuples [23] that can be directly used for experimental studies at the LHC. Each event is stored with additional matrix-element and PDF information to allow on-the-fly reweighting for different scale and PDF choices [26]. A user-friendly program, called HEPlot, is available to obtain predictions from these Ntuples for user-defined observables and kinematical cuts, including a thorough assessment of the uncertainties stemming from scale and PDF dependence. The Ntuple files are available upon request to the authors.

3. NLO predictions for the LHC at 13 TeV

We present selected results of interest for the LHC Run 2. Our predictions are based on the following set of cuts:

$$
\begin{aligned}
p_{\mathrm{T},\ell} &> 30~\mathrm{GeV}\,, & p_{\mathrm{T},b} &> 40~\mathrm{GeV}\,, & p_{\mathrm{T}}^{\mathrm{miss}} &> 50~\mathrm{GeV}\,,\\
\Delta R_{\ell b} &> 0.4\,, & \Delta R_{bb} &> 0.4\,, & \Delta R_{\ell\ell} &> 0.4\,,\\
|y_\ell| &< 2.5 & |y_b| &< 2.5\,,
\end{aligned}
\tag{3.1}
$$

where b, ℓ denote respectively any b-jet and charged lepton. We require exactly two b-jets, two charged leptons and missing p_{T} in the final state. Jets are defined according to the anti-k_{T} clustering algorithm [37] with resolution parameter $R = 0.4$.

With the goal of finding an optimal scale choice for the modeling of our observables, we have considered five different prescriptions:

$$\mu_0 = m_t + m_Z/2\,, \tag{3.2}$$
$$\mu_0 = H_{\mathrm{T}}/3 = \left(p_{\mathrm{T},e^+} + p_{\mathrm{T},\mu^-} + p_{\mathrm{T},b} + p_{\mathrm{T},\bar{b}} + p_{\mathrm{T}}^{\mathrm{miss}}\right)/3\,, \tag{3.3}$$
$$\mu_0 = E_{\mathrm{T}}/3 = \left(m_{\mathrm{T},t} + m_{\mathrm{T},\bar{t}} + p_{\mathrm{T},Z}\right)/3\,, \tag{3.4}$$
$$\mu_0 = E'_{\mathrm{T}}/3 = \left(m_{\mathrm{T},t} + m_{\mathrm{T},\bar{t}} + m_{\mathrm{T},Z}\right)/3\,, \tag{3.5}$$
$$\mu_0 = E''_{\mathrm{T}}/3 = \left(m_{\mathrm{T},t} + m_{\mathrm{T},\bar{t}}\right)/3\,, \tag{3.6}$$

where $m_{\mathrm{T},i} = \sqrt{p_{\mathrm{T},i} + m_i^2}$. We will refer to Eq. (3.2) as to our *fixed* scale choice, while the remaining ones are *dynamical* scales (*i.e.* phase-space dependent). The prescription of Eq. (3.3) makes use of the final-state momenta and is blind to any possible intermediate resonance, while Eqs. (3.4)–(3.6) make use of the momenta of the intermediate top quarks and Z bosons reconstructed with flavor information.

In Table I, we report our findings for the integrated cross section of the process $pp \to b\bar{b}e^+\nu_e\mu^-\bar{\nu}_\mu\nu_\tau\bar{\nu}_\tau + X$ as obtained with different scales and PDF sets. The complete cross section for the dilepton channel ($\ell = e, \mu$)

TABLE I

Integrated cross section of the process $pp \to b\bar{b}e^+\nu_e\mu^-\bar{\nu}_\mu\nu_\tau\bar{\nu}_\tau + X$ at $\sqrt{s} = 13$ TeV, as obtained with different scale and PDF choices. The reported errors denote theoretical uncertainties as obtained from scale variation. The last column reports the difference among various PDF sets.

σ^{NLO} [fb]	CT14	MMHT2014	NNPDF3.0	δ_{PDF}
$\mu_0 = m_t + m_Z/2$	$0.1266\,^{+1,1\%}_{-5.9\%}$	$0.1275\,^{+1.1\%}_{-5.9\%}$	$0.1309\,^{+1.1\%}_{-6.0\%}$	3.4%
$\mu_0 = H_{\mathrm{T}}/3$	$0.1270\,^{+0.7\%}_{-6.8\%}$	$0.1278\,^{+0.7\%}_{-7.0\%}$	$0.1312\,^{+0.7\%}_{-6.9\%}$	3.3%
$\mu_0 = E_{\mathrm{T}}/3$	$0.1272\,^{+1.6\%}_{-6.8\%}$	$0.1279\,^{+1.6\%}_{-6.8\%}$	$0.1313\,^{+1.6\%}_{-6.9\%}$	3.2%
$\mu_0 = E'_{\mathrm{T}}/3$	$0.1268\,^{+1.5\%}_{-6.4\%}$	$0.1280\,^{+1.5\%}_{-6.4\%}$	$0.1315\,^{+1.5\%}_{-6.5\%}$	3.7%
$\mu_0 = E''_{\mathrm{T}}/3$	$0.1286\,^{+1.0\%}_{-4.7\%}$	$0.1295\,^{+1.0\%}_{-4.7\%}$	$0.1330\,^{+1.0\%}_{-4.8\%}$	3.4%

can be obtained by multiplying the numbers in the table by a factor 12. The result is of the order of 1.5 fb and is comparable in size with typical expectations for DM signals (see *e.g.* Refs. [4–6]). We observe that cross sections based on different scale choices agree very well with each other. No substantial reduction of the scale uncertainties can be observed when using dynamical scales. This should not come as a surprise, since the importance of the dynamical scale does not lie in the calculation of the integrated cross section — a quite inclusive observable given our selection cuts — but rather manifests at a more exclusive level.

In the next step, we analyze a few differential cross sections relevant for phenomenological analyses. In Fig. 2, four different observables are shown: the variable $\cos\theta_{ll} = \tanh(\Delta\eta_{\ell\ell})$, the invariant mass between the two charged leptons (m_{ll}), the averaged transverse momentum of the charged leptons ($p_{\mathrm{T},l}$) and the transverse energy (H_{T}) defined as in Eq. (3.3). The first observable has been proven effective for determining the CP nature and mass of the DM mediator in simplified models [4]. It is crucial, to this end, a good control over the shape of the distribution other than a precise knowledge of the overall uncertainties. Looking at the $\cos\theta_{ll}$ distribution, one can see that the differential K-factor (middle panel) is far from being constant over the entire plotted range. The dynamical scales Eq. (3.3) and Eq. (3.6) perform better, yet shape distortions from LO to NLO up to $\mathcal{O}(15\%)$ can be observed in the tail of the distribution. Thus, for the observable at hand, the procedure of rescaling LO predictions by a global K-factor cannot guarantee reliable predictions as far as the shape is concerned and a full NLO calculation is recommended. Similar conclusions hold for the other observables reported in Fig. 2. We note, in particular in the cases of $p_{\mathrm{T},l}$ and H_{T}, that the fixed scale choice, Eq. (3.2), leads to NLO predictions which do not fit well within the LO uncertainty bands in the whole range. Here is where adopting dynamical scales shows its advantages in terms of improved perturbative stability, given that the process under consideration has an intricated structure of resonances and a genuine multi-scale nature.

Among all the infrared-safe observables that can be studied, the total missing transverse momentum ($p_{\mathrm{T}}^{\mathrm{miss}}$) plays a special role. The observation of an excess in $p_{\mathrm{T}}^{\mathrm{miss}}$ is indeed one of the most important signatures of DM and a very precise modeling is of course desirable. Our predictions for the $p_{\mathrm{T}}^{\mathrm{miss}}$ distribution are shown in Fig. 3. Looking at the middle panel, we note that results based on the fixed-scale choice exhibit the flattest K-factor. This behavior contrasts with the case of the observables previously examined, for which dynamical scales performed better. Typically, one expects that the fixed scale would describe more adequately the phase-space regions close to the threshold $m_{t\bar{t}} \approx 2m_t$, so a possible explanation of this behavior could be that contributions near threshold dominate the $p_{\mathrm{T}}^{\mathrm{miss}}$ distribution. We have checked, however, that this is not the case (see Fig. 4, left plot). To address

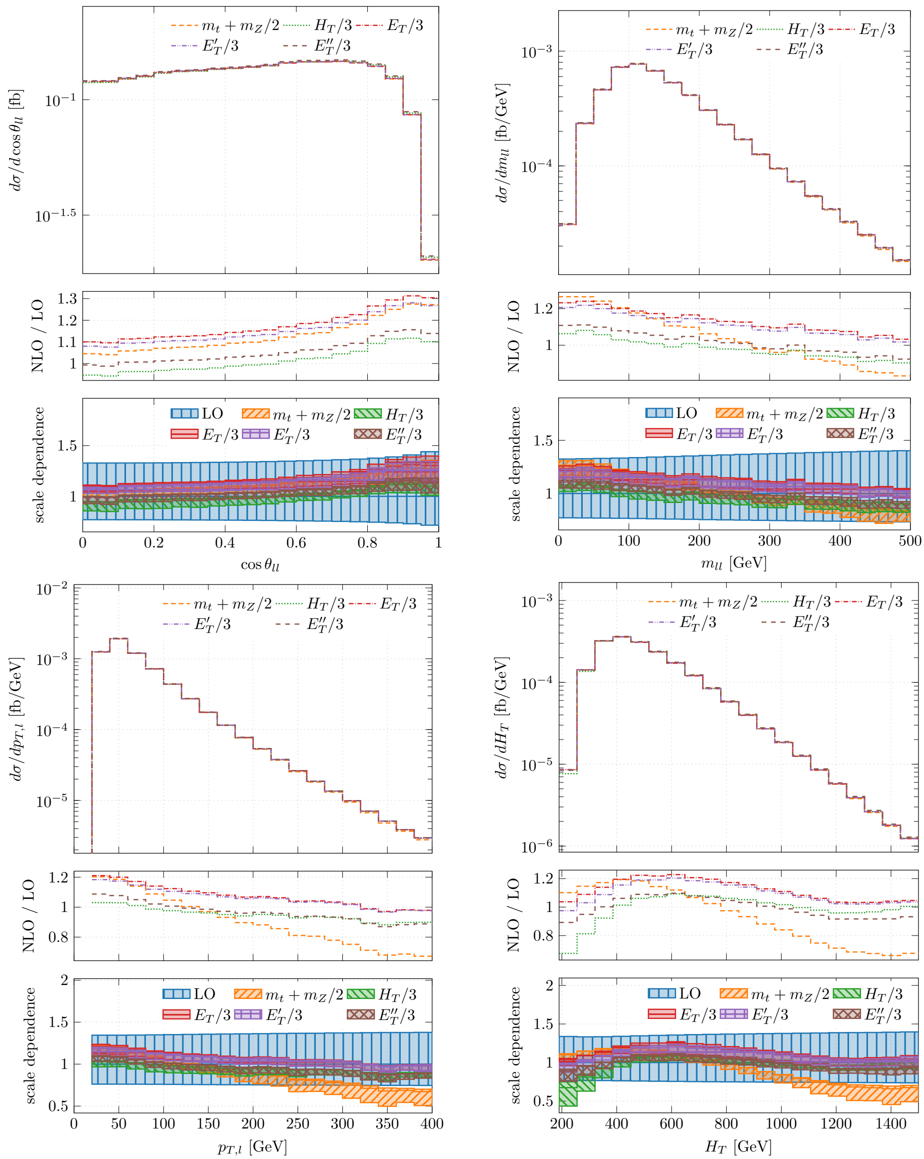

Fig. 2. Differential cross sections for $pp \to b\bar{b}e^+\nu_e\mu^-\bar{\nu}_\mu\nu_\tau\bar{\nu}_\tau + X$ as a function of $\cos\theta_{ll}$, m_{ll}, $p_{\mathrm{T},l}$ and H_{T} (defined in the text). Upper panels: absolute NLO QCD predictions for different scale choices. Middle panels: differential K-factors. Lower panels: uncertainty bands obtained from scale variation. The LO band refers to the scale choice $\mu_{\mathrm{R}} = \mu_{\mathrm{F}} = m_t + m_Z/2$. Results are based on the CT14 PDF set.

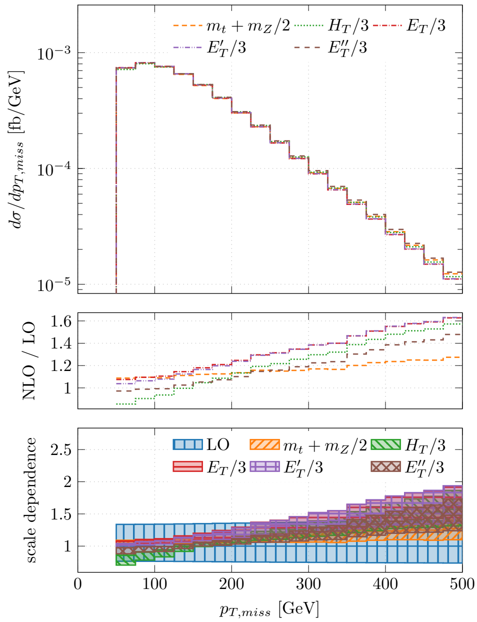

Fig. 3. Differential cross section for $pp \to b\bar{b}e^+\nu_e\mu^-\bar{\nu}_\mu\nu_\tau\bar{\nu}_\tau + X$ as a function of the total missing transverse momentum. The description is the same as for Fig. 2.

the interpretation of this behavior, we have examined the following two pseudo-observables: the transverse momentum of the ν_τ–$\bar{\nu}_\tau$ system ($p_{\mathrm{T},Z}$) and of the ν_e–$\bar{\nu}_\mu$ system ($p_{\mathrm{T}}^{\prime\,\mathrm{miss}}$). The first one corresponds to the p_{T} of the Z boson reconstructed from its invisible decay products, the second one is the missing p_{T} restricted to the neutrinos originated by top-quark decays. Although not directly measurable, these variables could help to shed light on the different behavior of the total missing p_{T} under fixed and dynamical scales. We note that the latter observable is not given as a simple sum of $p_{\mathrm{T},Z}$ and $p_{\mathrm{T}}^{\prime\,\mathrm{miss}}$ but rather as a convolution of some kind. Since the neutrinos involved in the definition of $p_{\mathrm{T},Z}$ and $p_{\mathrm{T}}^{\prime\,\mathrm{miss}}$ have different origin, we expect different kinematics for the two variables. This is somehow confirmed by Fig. 4 (right plot), which shows the NLO distributions of $p_{\mathrm{T}}^{\mathrm{miss}}$, $p_{\mathrm{T}}^{\prime\,\mathrm{miss}}$ and $p_{\mathrm{T},Z}$. The first two variables exhibit a softer p_{T} spectrum than $p_{\mathrm{T},Z}$, more specifically $\langle p_{\mathrm{T}}^{\prime\,\mathrm{miss}}\rangle < \langle p_{\mathrm{T}}^{\mathrm{miss}}\rangle < \langle p_{\mathrm{T},Z}\rangle$. In Ref. [3], we have explicitly checked that the behavior of $p_{\mathrm{T},Z}$ agrees with the other observables examined, namely it is better described by dynamical scales. On the other hand, for $p_{\mathrm{T}}^{\prime\,\mathrm{miss}}$ dynamical scales result typically in too large scale values and the fixed-scale choice is simply more adequate in the end, as for the case of the observable $p_{\mathrm{T}}^{\mathrm{miss}}$.

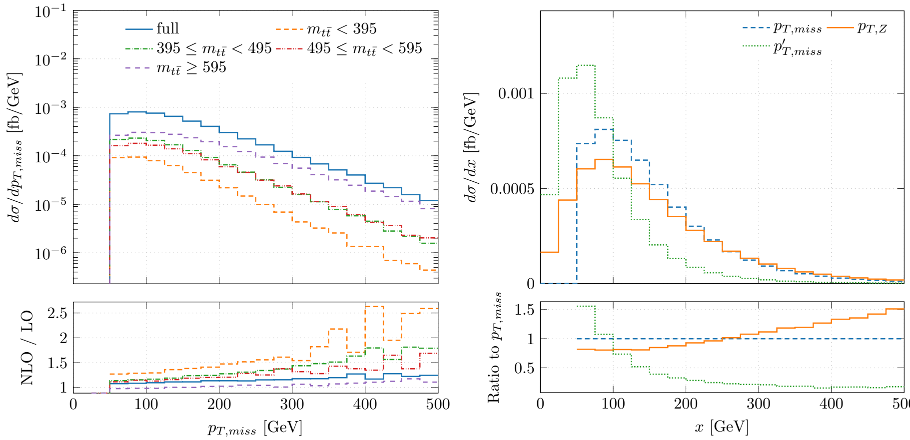

Fig. 4. Left plot: distribution of $p_{\rm T}^{\rm miss}$ for various ranges of $m_{t\bar{t}}$. Right plot: distributions of $p_{\rm T,miss}$, $p'_{\rm T,miss}$ and $p_{{\rm T},Z}$ (defined in the text). The upper panels show absolute NLO QCD predictions. The lower panels show ratios. Results are based on the scale $\mu_{\rm R} = \mu_{\rm F} = m_t + m_Z/2$ and on the CT14 PDF set.

4. Conclusions

We have presented the first full calculation of the SM process $pp \to b\bar{b}e^+\nu_e\mu^-\bar{\nu}_\mu\nu_\tau\bar{\nu}_\tau + X$ at NLO QCD accuracy. This provides the most complete description of the process of $t\bar{t}Z(Z \to \nu\bar{\nu})$ production in the dilepton channel at fixed perturbative order. We have discussed predictions for the LHC Run 2 at the energy of 13 TeV, with special emphasis on observables of interest for dark matter searches in the $t\bar{t} + E_{\rm T}^{\rm miss}$ channel. The theoretical uncertainty of the NLO cross section, as estimated from scale variation, is of the order of 6%, whereas PDF uncertainties are at the level of 3%. We have also examined a few differential cross sections, finding that QCD corrections induce relevant shape distortions. Given that a good control over shapes is a key in certain DM analyses, using full NLO predictions is important for a correct interpretation of the signals that may arise from the data. Furthermore, in the quest for an optimal scale choice for our predictions, we have found that $\mu_0 = H_{\rm T}/3$ and $\mu_0 = E''_{\rm T}/3$ ensure a good modeling for most of the observables examined. The total transverse momentum $p_{\rm T}^{\rm miss}$, however, turns out to be better described by the fixed scale $\mu_0 = m_t + m_Z/2$. We interpret this behavior as a consequence of the fact that our dynamical scale choices result in too large scales for this observable, as evinced from the analysis of the two pseudo-observables $p_T'^{\rm miss}$ and $p_{{\rm T},Z}$.

On the technical side, we remark that the results of our calculation are available in the form of event Ntuples. These might be directly used for experimental analyses at the LHC as well as to get accurate SM predictions in BSM studies, and are available under request.

The research of G.B. was supported by grant K 125105 of the National Research, Development and Innovation Office in Hungary.

REFERENCES

[1] C. Arina *et al.*, *J. High Energy Phys.* **1611**, 111 (2016).

[2] G. D'Ambrosio *et al.*, *Nucl. Phys. B* **645**, 155 (2002).

[3] G. Bevilacqua *et al.*, `arXiv:1907.09359 [hep-ph]`, accepted for publication in *J. High Energy Phys.*

[4] U. Haisch, P. Pani, G. Polesello, *J. High Energy Phys.* **1702**, 131 (2017).

[5] R. Boughezal, M. Schulze, *Phys. Rev. Lett.* **110**, 192002 (2013).

[6] R. Boughezal, M. Schulze, *Phys. Rev. D* **88**, 114002 (2013).

[7] A. Lazopoulos *et al.*, *Phys. Lett. B* **666**, 62 (2008).

[8] R. Röntsch, M. Schulze, *J. High Energy Phys.* **140**, 091 (2014) [*Erratum ibid.* **1509**, 132 (2015)].

[9] M.V. Garzelli, A. Kardos, C.G. Papadopoulos, Z. Trocsanyi, *Phys. Rev. D* **85**, 074022 (2012).

[10] S. Frixione *et al.*, *J. High Energy Phys.* **1506**, 184 (2015).

[11] O. Bessidskaia Bylund *et al.*, *J. High Energy Phys.* **1605**, 052 (2016).

[12] A. Kulesza *et al.*, *Eur. Phys. J. C* **79**, 249 (2019).

[13] A. Broggio *et al.*, *J. High Energy Phys.* **1704**, 105 (2017).

[14] G. Ossola, C.G. Papadopoulos, R. Pittau, *Nucl. Phys. B* **763**, 147 (2007).

[15] G. Ossola, C.G. Papadopoulos, R. Pittau, *J. High Energy Phys.* **0803**, 042 (2008).

[16] A. van Hameren, *Comput. Phys. Commun.* **182**, 2427 (2011).

[17] G. Bevilacqua *et al.*, *Comput. Phys. Commun.* **184**, 986 (2013).

[18] A. van Hameren, C.G. Papadopoulos, R. Pittau, *J. High Energy Phys.* **0909**, 106 (2009).

[19] S. Catani, M.H. Seymour, *Nucl. Phys. B* **485**, 291 (1997) [*Erratum ibid.* **510**, 503 (1998)].

[20] S. Catani, S. Dittmaier, M.H. Seymour, Z. Trocsanyi, *Nucl. Phys. B* **627**, 189 (2002).

[21] A. van Hameren, `arXiv:1003.4953 [hep-ph]`.

[22] J. Alwall *et al.*, *Comput. Phys. Commun.* **176**, 300 (2007).

[23] I. Antcheva *et al.*, *Comput. Phys. Commun.* **180**, 2499 (2009).

[24] M. Czakon, C.G. Papadopoulos, M. Worek, *J. High Energy Phys.* **0908**, 085 (2009).

[25] G. Bevilacqua, M. Czakon, M. Kubocz, M. Worek, *J. High Energy Phys.* **1310**, 204 (2013).

[26] Z. Bern *et al.*, *Comput. Phys. Commun.* **185**, 1443 (2014).

[27] A. Denner, S. Dittmaier, *Nucl. Phys. Proc. Suppl.* **160**, 22 (2006).

[28] G. Bevilacqua *et al.*, *J. High Energy Phys.* **1102**, 083 (2011).

[29] G. Bevilacqua, H.B. Hartanto, M. Kraus, M. Worek, *Phys. Rev. Lett.* **116**, 052003 (2016).

[30] G. Bevilacqua, H.B. Hartanto, M. Kraus, M. Worek, *J. High Energy Phys.* **1611**, 098 (2016).

[31] G. Bevilacqua *et al.*, *J. High Energy Phys.* **1810**, 158 (2018).

[32] G. Bevilacqua *et al.*, *J. High Energy Phys.* **1901**, 188 (2019).

[33] J. Butterworth *et al.*, *J. Phys. G* **43**, 023001 (2016).

[34] S. Dulat *et al.*, *Phys. Rev. D* **93**, 033006 (2016).

[35] L.A. Harland-Lang *et al.*, *Eur. Phys. J. C* **75**, 204 (2015).

[36] R.D. Ball *et al.* [NNPDF Collaboration], *J. High Energy Phys.* **1504**, 040 (2015).

[37] M. Cacciari, G.P. Salam, G. Soyez, *J. High Energy Phys.* **0804**, 063 (2008).